ELSEVIER

Ultramicroscopy 54 (1994) 229–236

ultramicroscopy

Incommensurate modulation in minute crystals revealed by combining high-resolution electron microscopy and electron diffraction

Z.Q. Fu [a], D.X. Huang [a], F.H. Li [*,a], J.Q. Li [b], Z.X. Zhao [b], T.Z. Cheng [c], H.F. Fan [*,a,d]

[a] *Institute of Physics, Chinese Academy of Sciences, Beijing 100080, People's Republic of China*
[b] *National Laboratory for Superconductivity, Institute of Physics, Chinese Academy of Sciences, Beijing 100080, People's Republic of China*
[c] *Laboratory for Structure Research, University of Science and Technology of China, Hefei 230026, People's Republic of China*
[d] *Department of Physics, Zhongshan University, Guangzhou 510275, People's Republic of China*

Received 8 May 1993; accepted 21 October 1993

Abstract

Image processing combining high-resolution electron microscopy and electron diffraction is for the first time applied to the determination of incommensurate modulated structures. An image of a minute crystal of the high-T_c superconductor $Bi_2Sr_2CaCu_2O_x$ is averaged and then transformed to an image of the average structure by a deconvolution technique based on the principle of maximum entropy. The image resolution is then enhanced to about 1 Å by the direct-method phase extension. All the unoverlapped atoms and their modulation are clearly seen in the final image.

1. Introduction

It is well known that an incommensurate modulated structure can be described as a high-dimensional periodic structure [1]. In principle, methods of crystal structure analysis for ordinary three-dimensional periodic structures remain valid for incommensurate modulated structures. X-ray diffraction analysis is no doubt a reliable technique to determine three-dimensional as well as high-dimensional periodic structures [1,2], in case the crystal size is large enough. It was reported that electron diffraction analysis had been successfully applied to determine the incommensurate modulated structure of minute crystals [3,4] provided the basic structure, in which the unmodulated atoms are situated at their averaged positions, is known in advance. In such cases, phases of the structure factors for main reflections are treated as those calculated from the basic structure, while phases of the satellite reflections are obtained by direct-method phase extension developed in X-ray crystallography. In fact the phases of main reflections could not be calculated exactly from the basic structure, because main re-

* Corresponding authors.

0304-3991/94/$07.00 © 1994 Elsevier Science B.V. All rights reserved
SSDI 0304-3991(94)00013-D

flections of an incommensurate modulated structure are attributed to the corresponding average structure rather than the basic structure. Structure factors of the former are affected by the modulation. Obviously the stronger the modulation, the larger the deviation of the average structure from the basic structure. It is difficult to derive the average structure purely from diffraction data before the incommensurate modulated structure has been solved, but it is easy to obtain the average structure from a high-resolution electron microscope image. Therefore, for solving structures of minute crystals with strong modulation, it is important to combine information from both the electron microscope image and the corresponding electron diffraction patterns.

Image processing by combining high-resolution electron microscopy and electron diffraction provides an approach to crystal structure analysis [5–9]. The procedure is generally divided into two steps: image deconvolution and resolution enhancement. In principle either one of the two steps can be used to determine a crystal structure. When the initial image is not taken under the optimum defocus condition, the process of image deconvolution can transform the image into the structure image [10–17]. But the resolution of such an image is limited by the resolution of the electron microscope. If on the other hand one starts with an optimum defocus image, the task is to enhance the image resolution by phase extension using electron diffraction data [5–9,18,19]. However, it is difficult to find the optimum defocus image from a series of experimental images, if the crystal under examination is completely unknown. Moreover, it is often impossible to obtain a series of images with different defocus values when the sample is sensitive to electron beam irradiation. Therefore, two-step image processing including image deconvolution and resolution enhancement is more applicable and can lead to a better result than by using either of the two steps. The two-step procedure has been successfully applied to determine an unknown structure with ordinary three-dimensional periodicity [8]. In the present paper, the technique is extended to the study of the incommensurate modulation in minute crystals of the high-T_c superconducting phase, $Bi_2Sr_2CaCu_2O_x$. The one-dimensional incommensurate modulation of the crystal has been studied by different methods [20–23], all of which were based on the basic structure and some assumption on the form of modulation. In our present study, a high-resolution electron microscope image was used to derive the average structure, which provides a better basis for deriving the phases of main as well as satellite reflections. No prior information about the basic structure and structural modulation is needed in our work.

2. Experimental

The crystals were crushed in an agate mortar. The fine fractures were transferred to a copper grid covered with holey carbon film and examined with an H-9000NA electron microscope operating at 300 kV. A special series of [100] zone electron diffraction patterns with sharp satellite reflections were taken with different exposures for recording the electron diffraction intensities [8]. The high-resolution electron microscope image projected along the $\boldsymbol{a}$ axis was picked up, using a CCD camera, from the paper by Matsui and Horiuchi [24], which was taken with a JEM-4000EX electron microscope.

3. Crystallographic data from electron diffraction

It has been determined that the average structure belongs to the orthorhombic system with lattice parameters $a = 5.39$, $b = 5.40$ and $c = 30.6$ Å. The structure is one-dimensionally modulated with modulation vector $\boldsymbol{q} = 0.21\boldsymbol{b}^* + \boldsymbol{c}^*$. All the main satellite reflections can be indexed as $h_1h_2h_3h_4$ corresponding to a four-dimensional reciprocal lattice [25,26] with lattice vector expressed as

$$\boldsymbol{H} = h_1\boldsymbol{b}_1 + h_2\boldsymbol{b}_2 + h_3\boldsymbol{b}_3 + h_4\boldsymbol{b}_4,$$

where $\boldsymbol{b}_1 = \boldsymbol{a}^*$, $\boldsymbol{b}_2 = \boldsymbol{b}^*$, $\boldsymbol{b}_3 = \boldsymbol{c}^*$ and $\boldsymbol{b}_4 = \boldsymbol{q} + \boldsymbol{d}$, $\boldsymbol{d}$ is a unit vector perpendicular to all other three reciprocal basic vectors, $\boldsymbol{a}^*$, $\boldsymbol{b}^*$ and $\boldsymbol{c}^*$. The superspace group determined from the four-dimen-

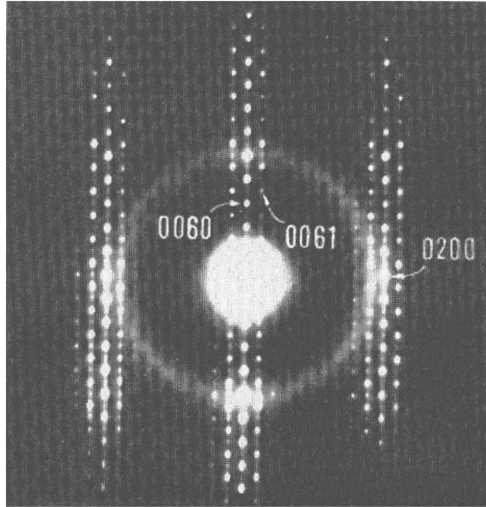

Fig. 1. Electron diffraction pattern of $Bi_2Sr_2CaCu_2O_x$ taken with the incident beam parallel to the *a* axis.

sional extinction rule is $N_{\bar{1}\bar{1}1}^{Bbmb}$ or $N_{\bar{1}\bar{1}1}^{Bb2b}$ [27]. Fig. 1 shows the electron diffraction pattern of the [100] zone. The high intensity of satellite reflections imply strong modulation and large deviation of the basic structure from the average structure.

4. Average structure image and image deconvolution

An average structure image is defined as the optimum defocus image of an incommensurate modulated structure averaged according to the unit cell of the basic structure. In the case that one does not start with an optimum defocus image, deconvolution should be done either before or after the image averaging. In our present study the latter approach was adopted. The image averaging was performed by dividing the image into many parts, each of which corresponds to a unit cell of the basic structure, and then summing up all parts of the image. The image deconvolution was carried out by making use of the maximum entropy principle [16]. According to the image contrast theory of weak-phase-object approximation in high-resolution electron microscopy, the image intensity is proportional to the convolution of the projected potential distribution function of the object with the inverse Fourier transform of the contrast transfer function:

$$I(\boldsymbol{r}) = 1 + 2\sigma\phi(\boldsymbol{r}) * \mathrm{FT}^{-1}[W(\boldsymbol{H})], \quad (1)$$

where $*$ and FT^{-1} are operators of convolution and inverse Fourier transform, respectively, $\sigma = \pi/\lambda U$, λ is the electron wavelength and U the accelerating voltage of electrons, $\phi(\boldsymbol{r})$ denotes the projected potential distribution function and $W(\boldsymbol{H})$ the contrast transfer function. The Fourier transform of Eq. (1) yields

$$T(\boldsymbol{H}) = \delta(\boldsymbol{H}) + 2\sigma F(\boldsymbol{H})W(\boldsymbol{H}), \quad (2)$$

where $T(\boldsymbol{H})$ denotes the Fourier transform of image intensities, $\delta(\boldsymbol{H})$ the Dirac delta function and $F(\boldsymbol{H})$ the structure factor which is the Fourier transform of $\phi(\boldsymbol{r})$. The simplest form of $W(\boldsymbol{H})$ is expressed as

$$W(\boldsymbol{H}) = \sin\,\chi_1(H)\,\exp[-\chi_2(H)], \quad (3)$$

where

$$\chi_1(H) = \pi\Delta f\lambda H^2 + \tfrac{1}{2}(\pi C_s\lambda^3H^4), \quad (4)$$

$$\chi_2(H) = \tfrac{1}{2}(\pi^2\lambda^2H^4D^2). \quad (5)$$

Here Δf is the defocus value, C_s is the spherical aberration coefficient and D is the standard deviation of the Gaussian distribution of defocus due to the chromatic aberration [28]. The values of Δf, C_s and D should be found before the image can be deconvoluted. C_s is nearly constant for a given electron microscope and can be determined experimentally [29]. The value of D can be set properly by experience. Besides, C_s and D do not change much for each image in contrast to Δf. Hence the main problem is to evaluate Δf. Eq. (2) can be rearranged to give

$$F(\boldsymbol{H}) = T(\boldsymbol{H})/2\sigma W(\boldsymbol{H}), \quad \boldsymbol{H} \neq 0. \quad (6)$$

According to Eq. (6), assuming C_s and D are known, given a trial value of Δf one can derive both amplitudes and phases of a set of trial $F(\boldsymbol{H})$ from the Fourier transform of image intensities, $T(\boldsymbol{H})$. A trial projected potential distribution function can then be calculated from the trial set of $F(\boldsymbol{H})$. Assigning values of the trial Δf in a wide range with small intervals, for instance 10 Å, a series of trial projected potential distribution functions can be obtained. Among these the cor-

rect one can be found by using the principle of maximum entropy. The entropy of the projected potential distribution function is defined as

$$S = -\sum_{i=1}^{N} p_i \ln p_i, \quad (7)$$

$$p_i = \phi_i / \sum_{i=1}^{N} \phi_i, \quad (8)$$

where ϕ_i denotes the value of projected potential of the ith pixel. Values of the entropy are calculated using (7) and (8) for all trial projected potential distribution functions. The one that is associated with the maximum value of entropy, is taken as the projected structure image. The above image deconvolution technique is based on the weak-phase-object approximation. Although in practice most samples are not weak phase objects, it was shown by the pseudo-weak-phase-object approximation [30] that Eq. (1) is valid in most cases. For crystalline samples with thickness under the critical value, deviation from the weak phase object leads mainly to corruption of the linear but not the monotonous relationship between atomic peak heights and the corresponding image intensities. The above image deconvolution technique has been proved to be effective for image simulation of chlorinated copper phthalocyanine [16] and for solving an unknown structure [8].

Fig. 2a shows the digitized image of $Bi_2Sr_2CaCu_2O_x$ projected along the ***a*** axis. In the image Bi atoms, which are the heaviest atoms in the crystal, appear black. This implies that the sample thickness is below the critical value and hence Eq. (1) is valid [30]. An area of size equal to $15\boldsymbol{b} \times 3\boldsymbol{c}$ from the image was averaged according to the unit cell of the basic structure to give an averaged image (Fig. 2b). This is then transformed into an image of the average structure (Fig. 2c) by an image deconvolution technique based on the principle of maximum entropy [16]. The resultant image represents the projection of the average structure along the ***a*** axis at a resolution of about 2 Å. As is seen the image resolution is not high enough even to distinguish all the metal atoms. However, the Fourier transform of Fig. 2c yields 17 phases of main reflections with spatial frequency up to 1.7 $Å^{-1}$. This provides a good basis for phase extension and refinement of main and satellite reflections as described in the next section.

5. Phase extension and refinement

A multi-dimensional direct-phasing method proposed by Hao, Liu and Fan [2] was used for phase extension and refinement of main reflections and then used for phase extension from

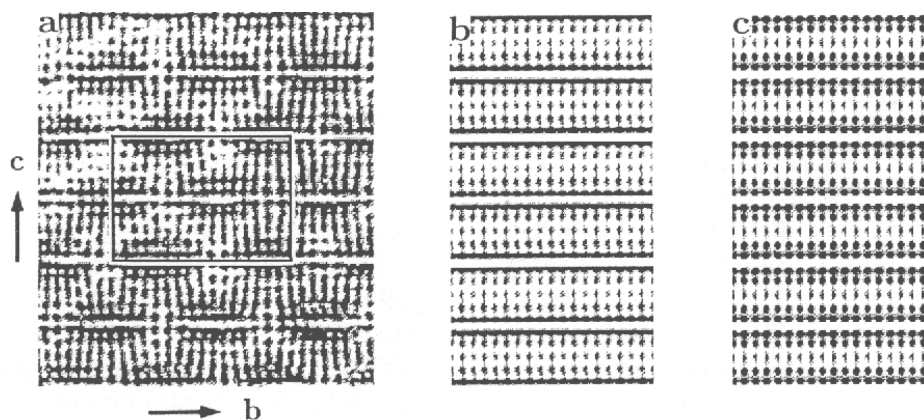

Fig. 2. High-resolution electron microscope images corresponding to Fig. 1. (a) Digitized from Ref. [24], (b) averaged from (a) according to the unit cell of the basic structure and (c) deconvoluted from (b).

main reflections to satellite reflections. A brief description of the method is given below.

A $(3+n)$-dimensional reciprocal lattice vector is expressed as

$$\hat{\boldsymbol{H}} = h_1\boldsymbol{b}_1 + h_2\boldsymbol{b}_2 + h_3\boldsymbol{b}_3 + \ldots + h_{3+n}\boldsymbol{b}_{3+n}, \quad (n = 1, 2, \ldots),$$

where $\boldsymbol{b}_i$ is the ith translation vector defining the reciprocal unit cell. h_i $(i = 1, 2, \ldots 3+n)$ are the integer indices of a reciprocal grid point corresponding to a reflection. In the present case, $i = 1$, 2, 3 and 4. The structure factor formula is written as

$$\boldsymbol{F}(\hat{\boldsymbol{H}}) = \sum_{j=1}^{N} f_j(\hat{\boldsymbol{H}}) \exp\left[\mathrm{i}2\pi\left(h_1\bar{x}_{j1} + h_2\bar{x}_{j2} + h_3\bar{x}_{j3}\right)\right], \quad (9)$$

where

$$f_j(\hat{\boldsymbol{H}}) = f_j(\boldsymbol{H}) \int_0^1 \times \mathrm{d}\bar{x}_4 \ldots \int_0^1 \mathrm{d}\bar{x}_{3+n} P_j(\bar{x}_4, \ldots, \bar{x}_{3+n}) \times \exp\left\{\mathrm{i}2\pi\left[\left(h_1U_{j1} + h_2U_{j2} + h_3U_{j3}\right) + \left(h_4x_{j4} + \ldots + h_{3+n}x_{j(3+n)}\right)\right]\right\}. \quad (10)$$

$f_j(H)$ on the right-hand side of (10) is the ordinary atomic scattering factor; P_j is the occupational modulation function; U_j describes the deviation of the jth atom from its average position. For more details on (9) and (10) the reader is referred to the original paper [2]. What should be emphasized here is that, according to (9), a modulated structure can be regarded as a set of "modulated atoms" situated at their average positions in three-dimensional space. The "modulated atom" in turn is defined by a "modulated atomic scattering factor" expressed as (10). With this description, we have the Sayre equation in multi-dimensional space:

$$\boldsymbol{F}(\hat{\boldsymbol{H}}) = \left(\theta(\hat{\boldsymbol{H}})/V\right) \sum_{\hat{H}'} \boldsymbol{F}(\hat{\boldsymbol{H}}')\boldsymbol{F}(\hat{\boldsymbol{H}} - \hat{\boldsymbol{H}}'), \quad (11)$$

where $\theta(\hat{\boldsymbol{H}})$ is an atomic form factor and V is the unit cell volume of the three-dimensional basic structure. The right-hand side of (11) can be split into three parts, i.e.

$$\boldsymbol{F}(\hat{\boldsymbol{H}}) = \left(\theta(\hat{\boldsymbol{H}})/V\right)\left[\sum_{\hat{H}'} \boldsymbol{F}_{\mathrm{m}}(\hat{\boldsymbol{H}}')\boldsymbol{F}_{\mathrm{m}}(\hat{\boldsymbol{H}} - \hat{\boldsymbol{H}}') + 2\sum_{\hat{H}'} \boldsymbol{F}_{\mathrm{m}}(\hat{\boldsymbol{H}}')\boldsymbol{F}_{\mathrm{s}}(\hat{\boldsymbol{H}} - \hat{\boldsymbol{H}}') + \sum_{\hat{H}'} \boldsymbol{F}_{\mathrm{s}}(\hat{\boldsymbol{H}}')\boldsymbol{F}_{\mathrm{s}}(\hat{\boldsymbol{H}} - \hat{\boldsymbol{H}}')\right]. \quad (12)$$

The subscript m stands for main reflections while the subscript s stands for satellites. Since the intensity of satellites are in average much weaker than that of main reflections, the last summation on the right-hand side of (12) is negligible in comparison with the second, while the last two summations on the right-hand side of (12) are negligible in comparison with the first. Now let $\boldsymbol{F}(\hat{\boldsymbol{H}})$ on the left-hand side of (12) represent only the structure factors of main reflections, we have to the first approximation

$$\boldsymbol{F}_{\mathrm{m}}(\hat{\boldsymbol{H}}) \simeq \left(\theta(\hat{\boldsymbol{H}})/V\right) \sum_{\hat{H}'} \boldsymbol{F}_{\mathrm{m}}(\hat{\boldsymbol{H}}')\boldsymbol{F}_{\mathrm{m}}(\hat{\boldsymbol{H}} - \hat{\boldsymbol{H}}'). \quad (13)$$

On the other hand, if $\boldsymbol{F}(\hat{\boldsymbol{H}})$ on the left-hand side of (12) corresponds only to satellites, it follows that

$$\boldsymbol{F}_{\mathrm{s}}(\hat{\boldsymbol{H}}) \simeq 2\left(\theta(\hat{\boldsymbol{H}})/V\right) \sum_{\hat{H}'} \boldsymbol{F}_{\mathrm{m}}(\hat{\boldsymbol{H}}')\boldsymbol{F}_{\mathrm{s}}(\hat{\boldsymbol{H}} - \hat{\boldsymbol{H}}'). \quad (14)$$

Notice that in this case the first summation on the right-hand side of (12) will vanish, because any three-dimensional reciprocal lattice vector corresponding to a main reflection should have zero components in the extra dimensions, hence the sum of two such lattice vectors could never give rise to a lattice vector corresponding to a satellite. Eq. (13) provides the basis for ab-initio phase determination as well as phase extension and refinement involving only the main reflections. Eq. (14) can be used to derive phases of satellite reflections based on the known phases of main reflections. A multi-dimensional direct-method program [31] was written for applying

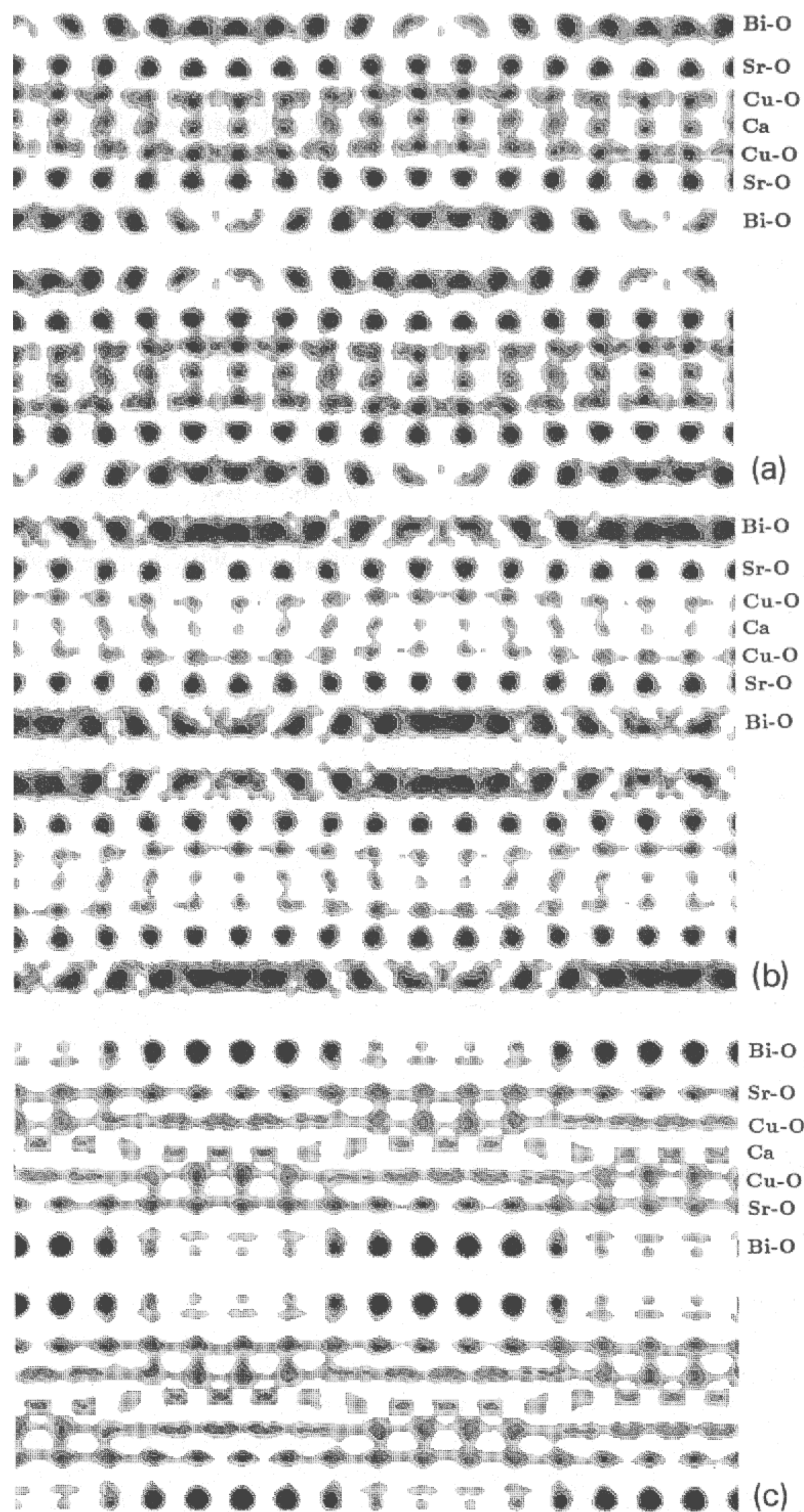

Fig. 3. Images obtained after direct-method phase extension. The initial phases of 17 main reflections are obtained from (a) the averaged image after deconvolution, (b) the averaged image without deconvolution and (c) the basic structure. They correspond in size to the framed area in Fig. 2a.

(13) and (14). The program has been tested with over ten known as well as originally unknown incommensurate modulated structures and was proved to be very efficient.

Phase extension and refinement were started with 17 phases of main reflections obtained from the image deconvolution. Eq. (13) was first applied to the main reflections. The starting phases were kept fixed during the first few cycles and allowed to change afterwards. By this manner phases of 21 additional main reflections with spatial frequency up to 1 $Å^{-1}$ were obtained, three starting phases (signs) were changed during the refinement. Phases of satellite reflections were then derived by making use of (14) based on the known phases of main reflections. 114 phases of satellite reflections were obtained. With the observed structure factor magnitudes and the phases obtained as above, a Fourier map (the potential distribution function projected along the ***a*** axis) was calculated (see Fig. 3a). This is actually the result from the image processing of Fig. 2a. The most prominent improvement in Fig. 3a is that there are more structural details at higher resolution. In between two Bi–O double layers Fig. 3a shows clearly five layers of atoms which correspond to the two Sr–O layers, two Cu–O layers and one Ca layer. These layers are not clearly seen in Fig. 2a, they are merged to give only three layers of black dots owing to the lens aberration and the limited resolution of the original electron micrograph. In addition all the atoms, except those overlapped due to projecting along the ***a*** axis, are well separated in Fig. 3a. Modulation waves of individual atoms are revealed intuitively and objectively.

6. Discussion

The main point in solving an incommensurate modulated structure by direct methods is on phasing the satellite reflections. This in turn is based on the known phases of main reflections. In theory, the phases of main reflections should correspond to the average structure, which bares the information of modulation. In practice there are different ways to obtain the phases of main reflections. In the present work the phases of main reflections were calculated through the Fourier transform of the deconvoluted averaged image. The latter is a good approximation to the true average structure. In the case that the image is taken near the optimum defocus condition, such as that of Fig. 2a, phases of main reflections can also be obtained through the Fourier transform of the averaged image without deconvolution. The resultant map based on this approach is shown in Fig. 3b, the quality of which is acceptable but atoms other than Bi and Sr are not as clearly revealed as in Fig. 3a. This means that even for an image taken near the optimum defocus condition, deconvolution is inevitable for obtaining a good-quality image. If on the other hand there is no structural image available, the phases of main reflections are usually derived from a so-called basic structure instead of the average structure. The former is obtained from an ordinary three-dimensional structure analysis using only the intensities of main reflections. The theoretical basis for this is the assumption that the basic structure is a good approximation to the average structure. Such an assumption is valid only when the modulation is weak. Otherwise the phases obtained for main reflections will differ considerably from those of the true average structure. This will affect the resultant phases of satellite reflections and degrade the final image. An example can be seen from Fig. 3c, which is obtained in the same way as Fig. 3a except that the starting phases of main reflections were calculated from the basic structure [21]. In conclusion, the combination of electron diffraction analysis with electron microscopy is important for solving strongly modulated structures.

Acknowledgements

The authors H.F.F. and F.H.L. are indebted to Drs. Y. Matsui and S. Horiuchi for kindly allowing the use of the electron microscope image of the Bi-2212 superconductor (Fig. 2a). This project is supported in part by the National Natural Science Foundation of China.

References

[1] P.M. de Wolff, Acta Cryst. A 30 (1974) 777.
[2] Q. Hao, Y.W. Liu and H.F. Fan, Acta Cryst. A 43 (1987) 820.
[3] S.B. Xiang, H.F. Fan, X.J. Wu, F.H. Li and Q. Pan, Acta Cryst. A 46 (1990) 929.
[4] Y.D. Mo, T.Z. Cheng, H.F. Fan, J.Q. Li, B.D. Sha, C.D. Zheng, F.H. Li and Z.X. Zhao, Phys. Scr. T 42 (1992) 18.
[5] H.F. Fan and F.H. Li, Direct Methods, Macromolecular Crystallography and Crystallographic Statistics (World Scientific, Singapore, 1987) pp. 400–409.
[6] F.H. Li, Int. Symp. on Electron Microscopy (World Scientific, Singapore, 1990) pp. 300–316.
[7] H.F. Fan, S.B. Xiang, F.H. Li, Q. Pan, N. Uyeda and Y. Fujiyoshi, Ultramicroscopy 36 (1991) 361.
[8] J.J. Hu, F.H. Li and H.F. Fan, Ultramicroscopy 41 (1992) 387.
[9] W. Dong, T. Baird, J.R. Fryer, C.J. Gilmore, D.D. MacNicol, G. Bricogne, D.J. Smith, M.A. O'Keefe and S. Hovmöller, Nature 355 (1992) 605.
[10] P.N.T. Unwin and R. Henderson, J. Mol. Biol. 94 (1975) 425.
[11] A. Klug, Chem. Scr. 14 (1978/1979) 245.
[12] F.H. Li and H.F. Fan, Acta Phys. Sin. 28 (1979) 276.
[13] F.S. Han, H.F. Fan and F.H. Li, Acta Cryst. A 42 (1986) 353.
[14] S. Hovmöller, A. Sjögren, G. Farrants, M. Sundberg and B.-O. Marinder, Nature 311 (1984) 238.
[15] N. Uyeda and K. Ishizuka, in: Proc. 8th Int. Congr. on Electron Microscopy, Canberra, 1974, Vol. 1, p. 322.
[16] J.J. Hu and F.H. Li, Ultramicroscopy 35 (1991) 339.
[17] D. van Dyck, in: Proc. 10th Eur. Congr. on Electron Microscopy, Granada, Spain, 1992, Vol. 1, p. 149.
[18] K. Ishizuka, M. Miyazaki and N. Uyeda, Acta Cryst. A 38 (1982) 408.
[19] H.F. Fan, Z.Y. Zhong, C.D. Zheng and F.H. Li, Acta Cryst. A 41 (1985) 163.
[20] Y. Gao, P. Lee, P. Coppens, M.A. Subramanian and A.W. Sleight, Science 241 (1988) 954.
[21] A. Yamamoto, M. Onoda, E. Takayama-Muromachi, F. Izumi, T. Ishigaki and H. Asano, Phys. Rev. B 42 (1990) 4228.
[22] V. Petricek, Y. Gao, P. Lee and P. Coppens, Phys. Rev. B 42 (1990) 378.
[23] X.B. Kan and S.C. Moss, Acta Cryst. B 48 (1992) 122.
[24] Y. Matsui and S. Horiuchi, Jpn. J. Appl. Phys. 27 (1988) L2306.
[25] P.M. de Wolff, T. Janssen and A. Janner, Acta Cryst. A 37 (1981) 625.
[26] A. Janner, T. Janssen and P.M. de Wolff, Acta Cryst. A 39 (1983) 658.
[27] J.Q. Li, C. Chen, D.Y. Yang, F.H. Li, Y.S. Yao, Z.Y. Ran, W.K. Wang and Z.X. Zhao, Z. Phys. B (Cond. Matter) 74 (1989) 165.
[28] P.L. Fejes, Acta Cryst. A 33 (1977) 109.
[29] O.L. Krivanek, Optik 45 (1976) 97.
[30] F.H. Li, and D. Tang, Acta Cryst. A 41 (1985) 376.
[31] Z.Q. Fu and H.F. Fan, J. Appl. Cryst. (1994) in press.